Cross Strip Readout Detectors for High Time Resolution Imaging in the 120nm to 900nm Wavelength Regime

Oswald H.W. Siegmund, John V. Vallerga, Jason McPhate, Barry Welsh, Anton Tremsin,
Space Sciences Laboratory, U.C. Berkeley

ABSTRACT

Detectors with cross strip anodes have been used in open face and sealed tube detectors for detection of particles and light. In combination with high resolution position encoding electronics these have the capability of being able to independently record the accurate time and position of each detected photon event. Sealed tube (18 mm) microchannel plate cross strip anode detectors with supergen-II photocathodes, and open face cross strip anode detectors up to 40mm have been commissioned. These have high spatial resolution ($\leq$ 30 µm), are capable of high counting rates (input rates > 5 MHz), demonstrate time tagging of events with ~1.5 ns accuracy, and provide extended lifetimes. Related developments of high efficiency GaN photocathodes and novel MCP structures capable of providing 20 x 20 cm devices potentially enhance the applicability of these devices.

Keywords: Microchannel plate, photon counting, imaging, timing

1. INTRODUCTION

Microchannel plate (MCP) imaging detector schemes have found extensive uses in many fields from space applications [1-5], ground based astronomy [6], biology [7, 9], and night time reconnaissance [8] to synchrotron excited photoelectron emission spectroscopy [10]. We have made considerable advances with a new generation of MCP detector using the Cross Strip (XS) anode readout, and in development of microchannel plates and photocathodes. The XS anode uses charge division, and centroiding of microchannel plate charge signals detected on two orthogonal layers of sense strips to encode event X-Y positions, and event times. Two types of device have been constructed, open face schemes for use in short wavelength and particle detection applications, and a sealed tube configuration with a proximity focus SuperGen-II photocathode for visible light sensing. The operational detector scheme is shown in Fig. 1. In the case of sealed tube devices the radiation passes through the input window and is converted to photoelectrons by a photocathode, either on the inside of the window, or on the top MCP surface. Photoelectrons are amplified by a pair of MCPs with a gain of about 10^6 and are detected by a cross strip anode. Our development of the XS anode scheme has employed XS detectors with active areas of 18mm (open face and sealed tube), 25mm (open face) [11] and 40mm (open face) [12] using pairs of 6 micron pore microchannel plates. Since the gain required for XS readouts is an order of magnitude lower than other high resolution readouts, such as the cross delay line, this substantially increases the local counting rate capabilities and the overall lifetime.

To encode event positions we have built front end boards with 2x 32 channel preamplifier ASICs. The pre-amplified XS anode signals are post-amplified on the same board and sent to a parallel channel encoding system. The latter uses 50 Msps 12 bit ADCs that continuously digitize the signal for subsequent digital peak detection by an FPGA firmware implemented event position centroid calculation. This Parallel Cross Strip (PXS) electronics has allowed us to employ XS anodes with high spatial resolution at input event rates of >5 MHz with event timing of < 1.5 ns. Sealed tube XS detectors [13} with supergen-II photocathodes have demonstrated good spatial resolution (< 35 microns FWHM), image linearity and local counting rate capability (>200 events/MCP pore sec^{-1}) using low MCP gain (5 x 10^5) with the PXS electronics scheme. Background rates are dominated by the thermionic noise of the red sensitive photocathode. The 40 mm open face detector format has demonstrated < 20 micron FWHM resolution [12] and similar event rate performance. Meanwhile GaN photocathodes have been developed with high UV efficiency (>70%) and efficiency of ~20% in the 250-350 nm range. GaN photocathodes [14] up to 50mm have been tested with open face MCP detectors, and show good uniformity. A novel development of MCP fabrication technology [15] also promises to facilitate the development of strip readout detectors to large sizes (200 mm). Using borosilicate glass tubes, MCP substrates with 20 µm pores have been made in an 8" x 8" format. Smaller test pieces (33 mm) have been used to make working MCPs by depositing resistive, and electron emissive, layers by atomic layer deposition. Initial tests are very encouraging, with results similar to conventional MCPs.

Cross strip detectors have already been used for a number of applications including biological fluorescence lifetime imaging [9], space based instruments [11], and neutron imaging [16]. Detector systems using the developments described here may be a significant enabling technology for several important applications, including airborne and space situational awareness, high-speed adaptive optics, astronomy of transient and time-variable sources, and optical

metrology. Versions of our XS designs that can achieve < 1 ns time resolution will also be valuable for three-dimensional imaging, biological single-molecule fluorescence lifetime microscopy, optical and infrared tomography, and hybrid mass spectrometry.

2. CROSS STRIP DETECTOR SYSTEMS

2.1 Cross Strip Anodes and Detectors

The cross strip anode (XS) has a relatively coarse pattern, which we have most commonly implemented as a multi-layer metal and ceramic design on an alumina substrate (Fig. 2). The surface of the substrate has strip conductors on a ~0.6 mm period. Then sets of insulating and conducting fingers are applied in the orthogonal direction such that 50 % of the bottom layer is left exposed. The crosstalk between axes is kept small by placing buried ground strips between the two layers. The top and bottom strip conductors collect the charge from the MCPs with equal charge sharing between the axes. XS anodes constructed in this way are low outgassing, accommodate >800°C temperatures, and are compatible with sealed tube ultra high vacuum devices. The MCP charge cloud is matched to the anode period (~0.6 mm) so that charge is collected on several neighboring fingers to ensure an accurate event centroid can be determined [17]. XS anodes are mounted ~2.5 mm behind the MCPs and each strip is connected through a filled hermetic via to the back of the anode. The external connections are then routed, by a fan out, to a standard connector for the electronics outside the vacuum enclosure. Only two MCPs are needed since the electron gain required is 10^6, or less. Various anode geometries have been used including a 32 x 32 mm XS open face laboratory detector that demonstrated excellent resolution (<7 µm FWHM) at low MCP gain (~5 x 10^5) [17]. Detectors with anodes up to 50 x 50 mm format [17,18] have been made, and the smaller 22 mm format (Fig. 2) has been constructed for use in sealed tube detectors.
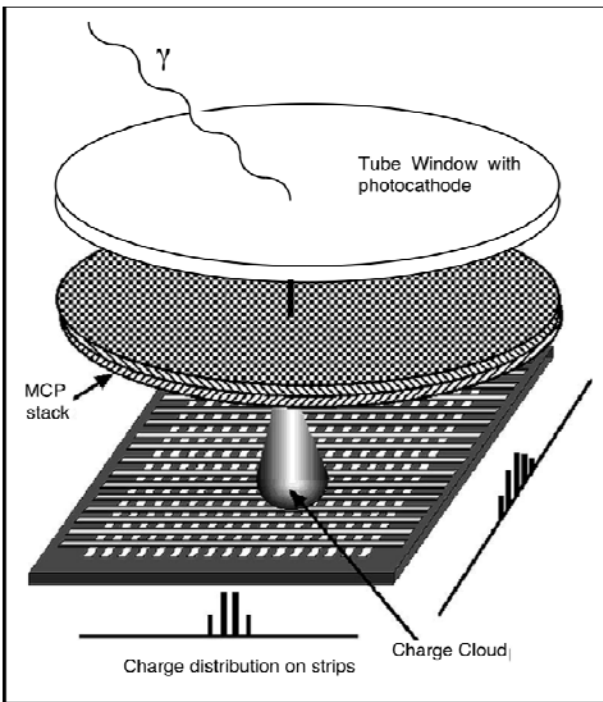

Fig. 1. Cross strip anode detector scheme. Light is detected by a photocathode on the entrance window, and the photo-electrons are amplified by an MCP pair and collected on several strips of each axis of the anode.
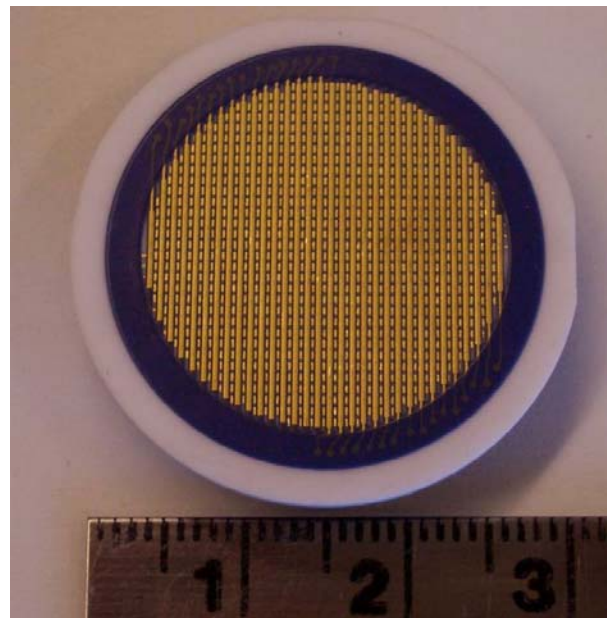
Fig. 2. 18 mm cross strip anode, showing the upper and lower strip layers each of which occupy ~50% of the area. Filled through hole vias allow the signals to be brought to back side for connections to the amplifiers.

2.2 Cross Strip Anode Sealed Tubes

The 22mm XS anode design (Fig. 2) is being used in open face [13] and in sealed tube MCP devices for sensing UV, and visible light respectively. A number of 18mm active area sealed tube detectors using the 22mm XS anode (Fig. 3) have been completed by Photonis. These have a SuperGen II photocathode deposited on the entrance window, which is proximity focused (<200 µm gap) to the input of a pair of MCPs. The MCPs have 6µm pores, 80:1 pore length to diameter ratio (L/d), 12 degree bias angle, and are placed in a back to back configuration. The XS anode is brazed to the back of the tube assembly and the distance between the anode and MCPs is ~2.5mm. We have used relatively low acceleration voltages of <100 V for the window gap and ~100 V for the anode gap. The MCPs used for most of these

tubes have relatively low resistance (<50 MΩ) which enables high local event counting rates to be achieved [13]. The SuperGenII photocathodes (Fig. 5) that were deposited by Photonis during tube fabrication have higher QE and redder response (Fig. 5) than the standard S20 photocathode tubes we have built previously. Three of the new 18mm tubes are currently being used for applications in biological fluorescence lifetime microscopy [9], while others have application in night-time remote sensing [13] and ground based astronomy [6]. There are also future plans to employ GaAs and GaAsP photocathodes in sealed tubes giving increased efficiency over two well defined wavelength ranges.

Fig. 3. 18 mm anode sealed tubes using the 22 mm cross strip anode shown in Fig. 2. Each tube has a MCP pair and a SuperGen-II photocathode providing a broad wavelength range coverage..

2.3 Cross Strip Event Encoding Electronics

Although the cross strip pattern is quite coarse, it is possible to find the position of each photon detected very accurately to a small fraction of the strip pitch. To derive the event positions we calculate the centroid of the charge cloud impinging on the XS anode strips in each axis. The first step is to attach each finger of an XS anode to a charge sensitive amplifier channel on a multi-channel amplifier chip. In our current parallel channel encoding scheme each strip on the anode is connected directly to a preamp input of a 2 x 32 channel ASIC (RD-20) amplifier board (Fig. 4)[13]. These preamplifiers produce unipolar pulses with ~40 ns rise time, and ~160 ns fall time with a measured noise of ~1000 e$^-$ RMS. The signals are buffer-amplified and sent via a coaxial ribbon cable to 64 (8 octal packs) analog to digital converters operating at 50 mega-samples per second. The digitized signal waveforms are read into an FPGA (Xilinx Virtex 5) using a LVDS serial stream. A custom filter is used to determine the peak charge [18] on the group of neighboring strips affected by an incident event, and corrections are applied to the data to account for amplifier gain variations, gain non-linearities, signal offsets and pedestals. The results are then used to derive the event centroid for both the X and Y axes. A coarse time tag (< 20ns) for each event is obtained using the FPGA clock counter. All the events are buffered and transferred to a downstream PC as an event list of X, Y and T for storage, and/or binning and display. The configuration of the electronics depends on the detector format used. The 22 mm XS anode (Fig. 4) as implemented in the 18 mm sealed tube (Fig. 2) requires only one RD20 board (2 x 32 channels) and one parallel cross strip (PXS) electronics system. In the case of our 40 mm XS detector [18] two RD20 amplifier boards and two PXS systems (one for X and one for Y) are required.

2.4 Cross Strip Detector Tests

The measured quantum efficiency of our photocathodes in the 18mm sealed tubes (Fig. 5) is typical of supergen-II photocathodes. This is considerably better than the S20 photocathodes we had used previously. Initial imaging tests with the detectors combined with the RD20/PXS electronics have been accomplished. To measure the spatial resolution and image linearity we project a resolution test mask image with small pinholes at regular intervals onto the photocathode (Fig. 6). The overall image linearity (Fig. 6) is quite good, with only the areas at the very edge of the image showing evidence of displacement from their true positions. The spatial resolution is dependent on a number of settings. One of the most important is the cathode proximity gap and the potential across it. An earlier test on one tube gave resolution as good as ~30 μm FWHM. The tube shown here used a comparatively low 75v proximity gap bias which gave ~50 μm FWHM resolution (Fig. 7). The behavior of the resolution as a function of event rate is highly dependent on the processing electronics setup. We can preserve the spatial resolution at high rates [13] by elimination,

and thus decreasing the overall throughput, of events that temporally overlap. In this case our 160 ns effective dead time results in reasonable throughput (~2 MHz), but as the event rate is increased to ~8 MHz input rate the spatial distribution blurs due to event pile-up, both spatially and temporally.
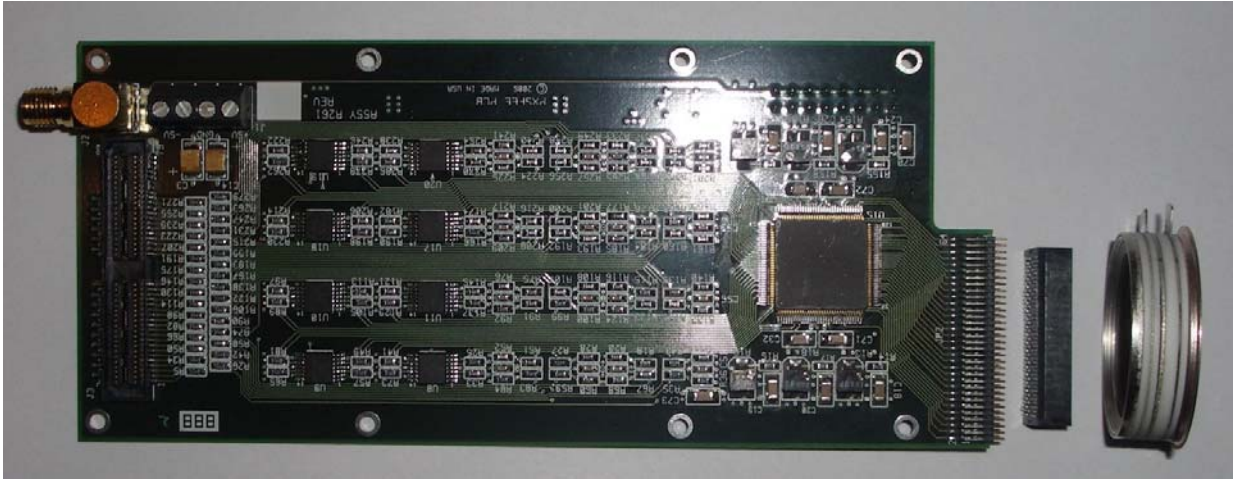

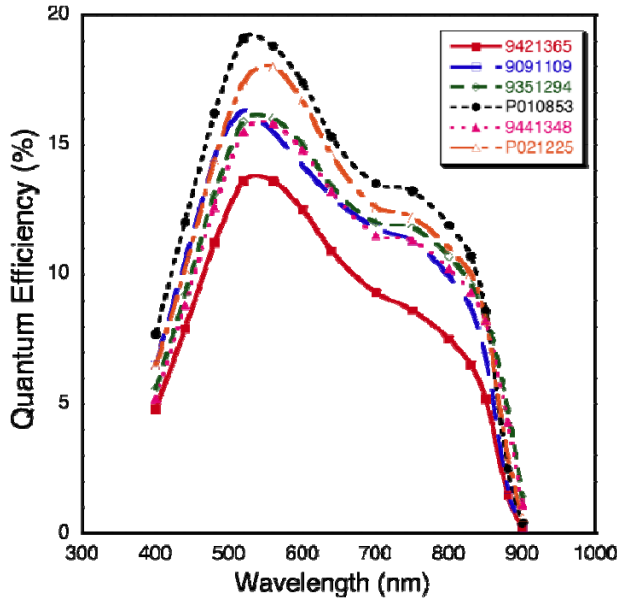Fig. 4. RD20 amplifier board shown with connector and 18mm sealed tube cross strip detector.

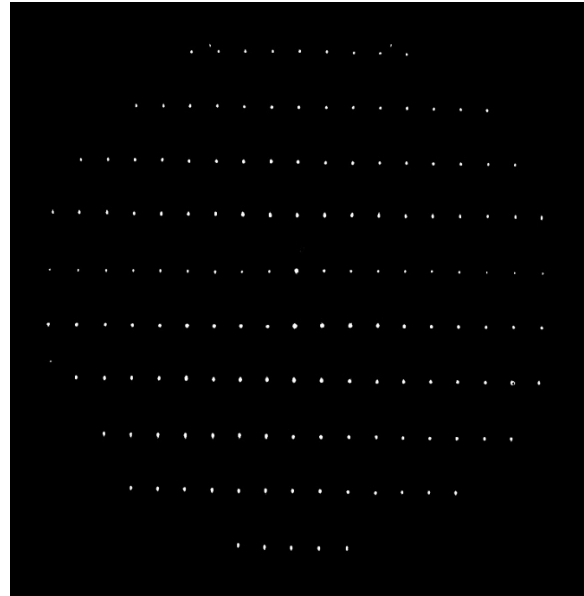Fig. 5. Photocathode quantum efficiency for 18 mm cross strip anode sealed tube detectors (SuperGen-II).

Fig. 6. Image of a projected spot array on an 18 mm cross strip tube. 1 mm X and 2mm Y spacing, 25 µm spots.

We are currently developing faster amplifiers and pulse shaping techniques to allow more rapid baseline restoration and hence higher counting rates with less effect on the resolution. The resolution results achieved with the sealed tubes is dominated by the proximity gap and the projected input point spread function. However, an open face detector with the same XS anode demonstrates ~17 µm FWHM (Fig. 8). The image in Fig. 8 clearly resolves the 40 µm wires of a grid mesh placed directly on the front face of the MCP. In the deep image shown it is also possible to see the very faint hexagonal modulation of the top and bottom MCPs.
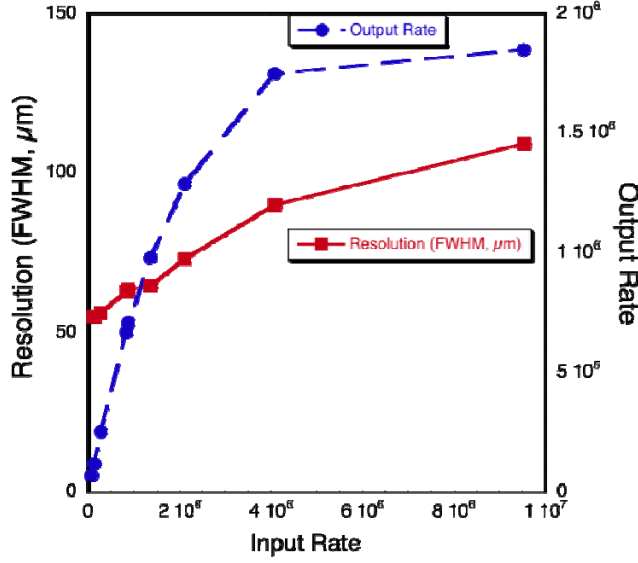
Fig. 7. Spatial resolution and electronics output count rate as a function of input event rate, 18mm XS tube. Electronics deadtime 160ns.
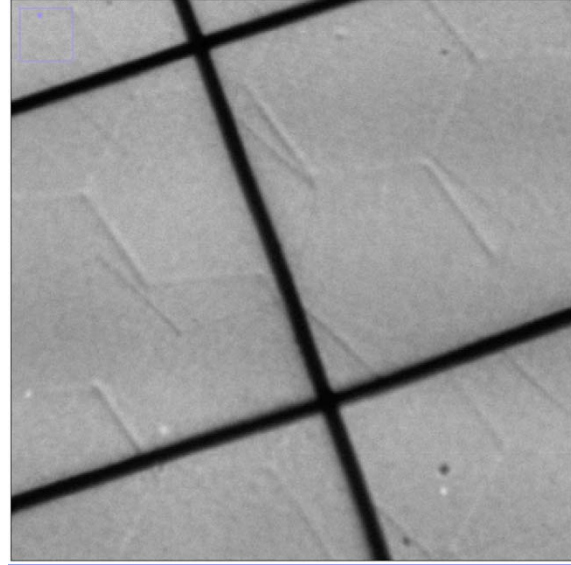

Fig. 8. High statistics image of a 2 mm area in an open face 18 mm cross strip detector. 1.2 mm period grid mask, 40 μm wires. 6 μm MCP pores, gain ~10^6, resolution ~17 μm FWHM.
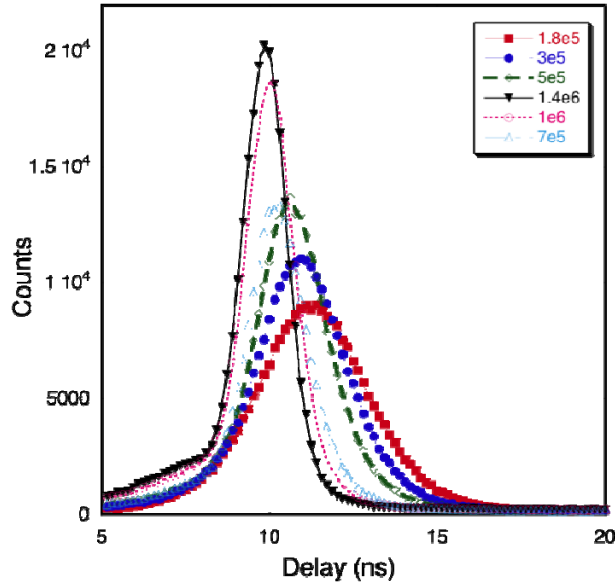

Fig.. 9. Event time stamp jitter distributions for PXS electronics. 18 mm cross strip tube, 80 ps jitter laser.
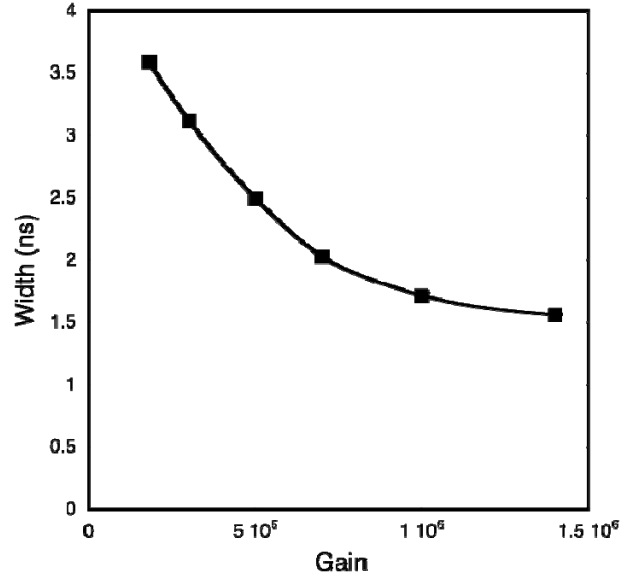

Fig.. 10. Event time stamp jitter (FWHM) as a function of event gain. 18 mm cross strip tube, 80 ps jitter laser.

2.5 Event Timing Characteristics

Several of the uses for the XS detectors require timing information for each event detected [19, 20]. The timing resolution required depends on the application, but can be as little as milli-seconds for astronomical applications, to nanoseconds for remote sensing and as little as 100 ps for biological fluorescence and synchrotron instruments. Simple time stamping of events with the FPGA clock time can accommodate those requiring resolution of 20 ns or greater. For more demanding timing applications there are a number of ways to establish better temporal resolution. The ultimate timing of the events depends on the intrinsic jitter in the processing of the detected photon by the MCP detector. From measured data this has the potential to be as good as ~25 ps, depending on a variety of physical setups, such as the proximity gaps, voltages, and others. A good way to achieve this is by examining the time of arrival of the MCP exit pulse with an amplifier attached to the bottom of the MCP, and a constant fraction discriminator, to compare the detected event time to the input source trigger. Since this requires a separate electronics channel it is not always

desirable to implement this configuration. For many of the uses that we are addressing we have used the inherent programmability of the FPGA to provide the event time stamp along with the event position centroid. This is achieved by effectively constructing a constant fraction discriminator applied to the 50 MHz digital pulse samples with the FPGA firmware. It can be applied to single or multiple strip channels of both axes for a given detected event. Initial tests of this approach (Fig. 9) with a pulsed laser show that the resulting timing jitter for the digital constant fraction timing interpolation is a Gaussian shape, as would be expected. As the gain of the detector is increased, the signal to noise improves and thus the width of the timing error distribution becomes narrower (Fig. 10). The 1.5 ns performance achieved is adequate for all but the most demanding applications.

We have also investigated the uniformity in the timing stamp as a function of position in the image by illuminating our detector with diffuse pulsed laser light (Fig. 11). We find that the temporal variations (Fig. 12) are of the order of 1ns and are distinctly related to the amplifiers/strips. Note that this is not a time jitter, but rather a fixed pattern timing offset that can be calibrated out. Generally the timing delay is smallest at the axis extremes, although there are variations for specific amplifiers/strips elsewhere. The inherent timing delay of the RD20 amplifiers varies due to pulse shape variations, with an increase in the pulse peak time of slightly less than 1ns/pF of increased load. The strips at the axis extremes are the shortest (Fig. 2) and are thus the strips with the smallest capacitive load for the amplifiers. This correlates well with the timing data of Fig. 12, and suggests that the strip features in Fig. 11 derive from small changes in the amplifier load. This characteristic indicates that future changes in amplifier design to minimize pulse shape changes will have a direct, and potentially significant, effect on the overall timing performance achieved.
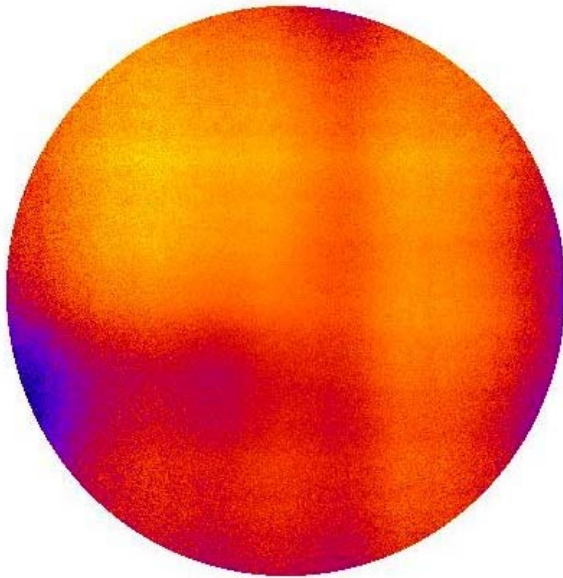

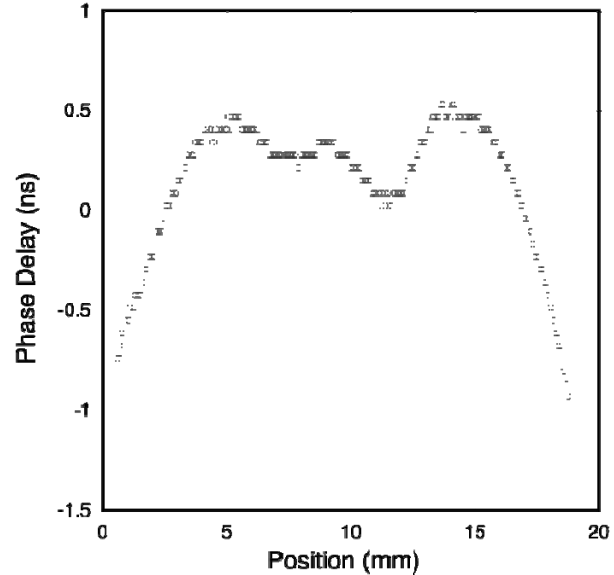Fig. 11: Image map of the variations in mean event arrival time across an 18mm cross strip sealed tube detector.

Fig. 12: Variation in the mean arrival time of events as v.s. position. Section of Fig. 11 along X in the center of Y.

3. BOROSILICATE - ATOMIC LAYER DEPOSITED MICROCHANNEL PLATES

There are many applications where large area detectors are needed, from imaging and spectroscopic sensors with a large number of small pixels for large space telescopes, to large numbers of large detectors with low spatial resolution but very high timing resolution for example in ring imaging Cherenkov detectors. The unique attributes of MCP detectors with strip anode readouts make them well suited for these applications, however, there are size limitations for current MCP fabrication and the costs for large areas become significant. For this reason a collaboration of University of Chicago, Argonne National Laboratory, University of California Berkeley, and several other universities and commercial concerns are exploring ways to develop a large (8" x 8") sealed photo-detector with microchannel plates that utilize a novel fabrication methodology [15].
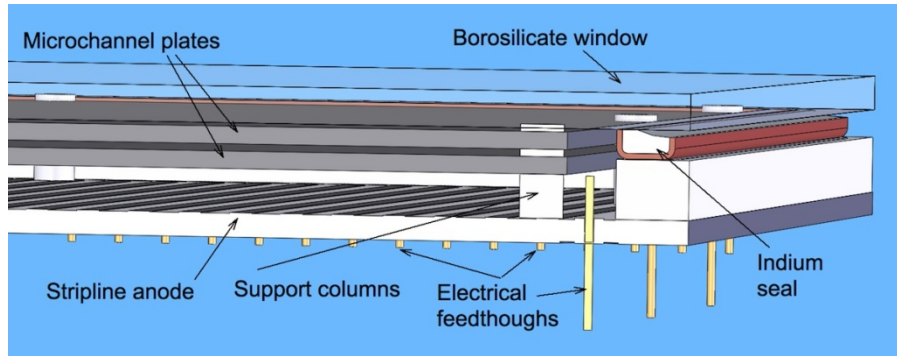
Fig. 13: Depiction of a cutaway of the design of a 8" x 8" sealed tube using large area borosilicate MCPs activated by atomic layer deposition, borosilicate entrance window with a bialkali photocathode, and stripline readout.

The large detector design (Fig. 13) being developed at the University of California Berkeley incorporates many conventional design concepts and materials. The overall assembly is an alumina brazed body with a hot indium sealed window. A vacuum transfer proximity focus bialkali photocathode on the inside of the window is used for photon conversion, and a pair of MCPs is used for amplification, depositing event charge onto a simple stripline anode. A similar concept, but with different construction techniques, is being developed by University of Chicago and Argonne National Laboratory. In both cases the MCPs represent a significant challenge due to their size. The operational requirements for the MCPs can be nominally met with MCP pore sizes of 20 µm, 60:1 L/d and a bias angle of 8 degrees, with two MCPs working as a biased gap pair. This provides sufficient gain ($>10^6$) with controllable charge cloud size to match the anode period, reasonable robustness with 1.2 mm thick MCPs and a configuration capable of achieving low time stamp jitter.
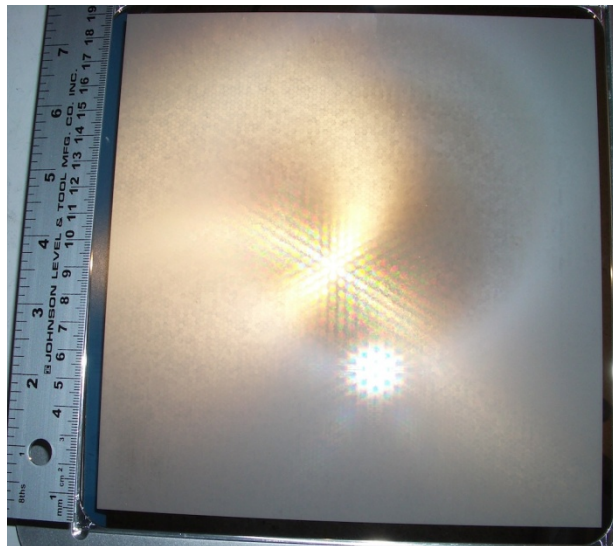

Fig. 14: 8" x 8" borosilicate substrate for MCP fabrication 20 µm pores, 8 degree bias, 60: 1 pore L/d.
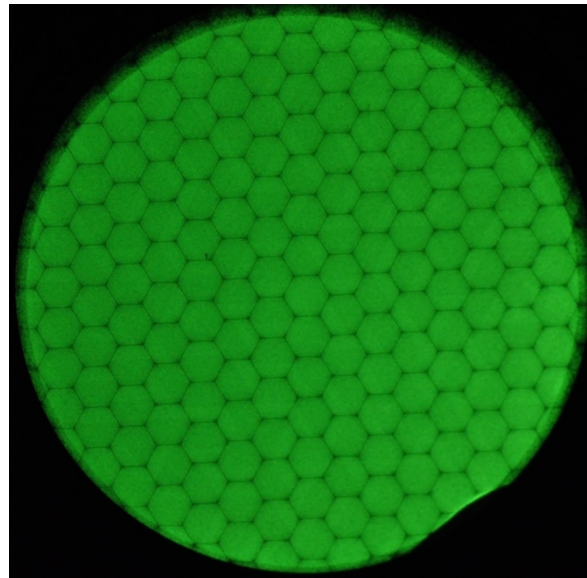
Fig. 15: 33 mm borosilicate/ALD MCP, 20 µm pores, 8° bias, 60: 1 pore L/d, 1200v. Phosphor screen readout.

The MCP construction scheme being investigated to produce 8" x 8" MCPs begins with borosilicate glass tubes with either hollow or filled cores. Borosilicate is a much more robust material than conventional MCP glasses, but does not have a chemical composition that is conducive to the chemical processing and hydrogen reduction that is applied to form the resistive and electron emissive surfaces on typical MCPs. It is also potentially considerably less costly. Using the borosilicate glass tubes the MCP substrate is made in a "nominally" conventional way by drawing and stacking the fibers. Incom Inc. have produced a number of substrates in 40 µm, and 20 µm pore sizes, with MCP formats of 32.7 mm, and most recently 8" x 8" (Fig. 14). The "activation" of the MCP surfaces is done using atomic layer deposition (ALD) [21]. Monolayers of resistive material are applied to the glass surfaces until the desired MCP top to bottom surface resistance is achieved. Then layers of high secondary emission coefficient material (Al_2O_3 for example) are applied by ALD along with top and bottom surface evaporated electrodes. Both Arradiance Inc. and Argonne National

Laboratory have successfully treated Incom 32.7 mm, 40 μm and 20 μm pore MCP substrates to produce working MCPs. We have tested some of these to establish the working parameters of this new process. As a baseline the gain, image uniformity, background, outgassing, dynamic range, thermal coefficient of resistance, and lifetime characteristics are all of interest. In addition for MCP pairs and stacks, the pulse amplitude distribution, intrinsic background event rate, and timing jitter issues are important. We have measured some of these qualities on both 40 μm [ref cassis] and 20 μm MCPs. The imaging of single 32.7 mm, 20 μm pore MCPs (Fig. 15) with a phosphor screen readout shows a significant amount of multi-fiber hexagonal modulation. This is a direct result of the deformation of the pores at the junction of the MCP multi-fiber bundles. This was common in conventional MCPs until fairly recently, and at this stage of development it is not surprising to have this issue, furthermore it is not necessarily problematic in some applications where timing is more important than imaging quality. Nevertheless, the overall image uniformity is quite flat, and there is an absence of any significant defects.
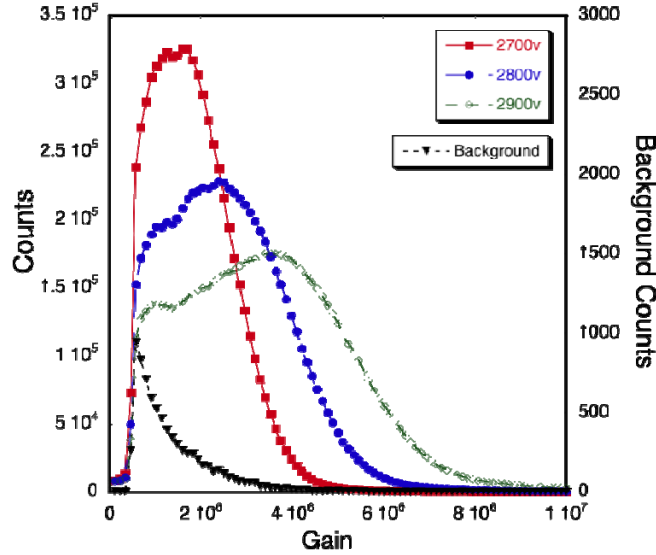

Fig. 16: Pulse amplitude distributions for an ALD processed borosilicate glass 20 μm pore MCP pair with 60:1 L/d each.
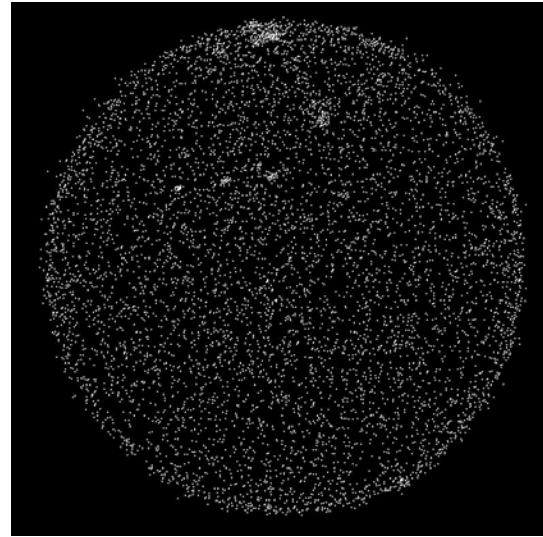
Fig. 17: Background event image for a 20 μm pore MCP pair, 25mm area, gain 2×10^6, ~1 event cm^{-2} sec^{-1}.

Tests with pairs of back-to-back stacked borosilicate MCPs [15] (Fig. 16) show peaked pulse amplitude distributions with gains up to ~5×10^6. The dark areas in Fig. 15 at the MCP multifiber boundaries are significantly lower in gain than the average. Thus the peaked gain distribution (Fig. 16) is not quite as well defined as it might otherwise be. The pulse risetimes for single photon detection by a pair of 20 μm MCPs is in the 1 ns range [ref], as observed for conventional MCPs. Single MCP gains of up to 10^5 have been achieved with 40 μm pore MCPs and >3 x 10^4 with 20 μm pore MCPs. The range of resistances achieved spans from <50 MΩ to more than 1 GΩ for 32.7 mm format MCPs. This is of great importance because the large 8" x 8" MCP resistance needs to be carefully chosen (~10 MΩ) to allow reasonable local area counting rates (lower resistances give better rate limits) while having an overall resistance that is not so low that the power requirement becomes prohibitively high, or even risks damaging the MCP. Background event rates for the 32.7 mm format MCP pairs are about 1 event cm^{-2} sec^{-1}, but show some "warm spots". The "warm spots" are probably due to issues with defects in the MCP construction. The new MCP materials also contain no lead and have minimal alkali metals, so the intrinsic background rate should be very low and the gamma ray detection efficiency should be much lower than the ~2% for conventional lead glass MCPs [22]. Initial life-tests of single MCPs [15] indicate a much shorter initial outgassing period than conventional MCPs, which may be an intrinsic benefit of the raw materials used for this new type of MCP. Our evaluations and studies of these MCPs show significant promise for several applications. Of note is that the MCPs have a sapphire (Al_2O_3) final ALD layer, and given the high temperature robustness of the borosilicate glass it makes the MCP a good candidate for deposition of GaN high efficiency (>70% @ 120 nm) UV photocathodes [14] directly on the front MCP surface. Verification of the detailed properties of the 32.7mm MCPs is in progress. Subsequently the large 8" x 8" MCPs will be processed and subjected to similar tests before the fabrication of sealed tubes is attempted.

4. ACKNOWLEDGEMENTS

5. REFERENCES

1. Siegmund, O.H.W., M.A. Gummin, J.M. Stock, et. al, Performance of the double delay line microchannel plate detect detectors for the Far-Ultraviolet-Spectroscopic Explorer, *Proc SPIE* 3114, pp.283-94, 1997.
2. Siegmund, O.H.W., P. Jelinsky, S. Jelinsky, et al., High resolution cross delay line detectors for the GALEX mission, *Proc. SPIE* 3765, pp.429-40, 1999.
3. Stock, J.M. O.H.W. Siegmund, J.S. Hull, et al.,Cross-delay-line microchannel plate detect detectors for the Spectrographic Imager on the IMAGE satellite, *Proc SPIE* 3445, pp.407-14, 1998.
4. Siegmund, O.H.W., M.A. Gummin, T. Sasseen, et al., Microchannel plates for the UVCS and SUMER instruments on the SOHO satellite*, Proc. SPIE* 2518, pp.334-55, 1995.
5. Vallerga, J.; Zaninovich, J.; Welsh, B.; Siegmund, O.; McPhate, J.; Hull, J.; Gaines, G.; Buzasi, D. The FUV detector for the cosmic origins spectrograph on the Hubble Space Telescope, *Nuclear Instruments and Methods in Physics Research Section A*, Volume 477, Issue 1-3, p. 551-555, 2002.
6. Siegmund, O.H.W., J. McPhate, A. Tremsin, J.V. Vallerga, B.Y. Welsh and J.M. Wheatley, *AIP Conference Proceedings*, 984, 103, 2008.
7. Siegmund, O.H.W., J. Vallerga, P. Jelinsky, M. Redfern, X. Michalet, S. Weiss, Cross Delay Line Detectors for High Time Resolution Astronomical Polarimetry and Biological Fluorescence Imaging, *IEEE* 2005 Nuclear Science Symposium and Medical Imaging Conference, Puerto Rico, October 2005.
8. Priedhorsky. W.and J. Bloch, *Applied Optics*, 44(3), 423-433, 2004.
9. Michalet, X.; Siegmund, O. H. W.; Vallerga, J. V.; Jelinsky, P.; Millaud, J. E.; Weiss, S., Photon-counting H33D detector for biological fluorescence imaging, Nuclear Instruments and Methods, A, Vol. 567(1), p. 133-136. 2006
10. Tremsin, A.S., G.V. Lebedev, O.H.W. Siegmund, et al, High spatial and temporal resolution photon/electron counting detector for synchrotron radiation research, *Nucl. Instrum. and Meth. A*, 580, 853-857, 2006.
11. Berendse, F. B., R. G. Cruddace, M. P. Kowalski, D. J. Yentis, W. R. Hunter, G. G. Fritz, O. Siegmund, K. Heidemann, R. Lenke, A. Seifert, T. W. Barbee, Jr. The joint astrophysical plasmadynamic experiment extreme ultraviolet spectrometer: resolving power, Proc. SPIE Vol. 6266, 62660V, 2006
12. Siegmund, O.H.W., Tremsin, Anton S., Vallerga, John V. Development of cross strip MCP detectors for UV and optical instruments, Proc. SPIE, Vol. 7435, p.14, 2009
13. Siegmund, O.H.W. John V. Vallerga, Anton S. Tremsin, Laura C. Stonehill, Robert Shirey, Michael W. Rabin, and David C. Thompson, Cross strip microchannel plate imaging photon counters with high time resolution, SPIE, Vol. 7681, p.768109, 2010.
14. Siegmund, O. H. W., Hull, J. S., Tremsin, A. S., McPhate, J. B., Dabiran, A. M., Gallium nitride photocathodes for imaging photon counters, Proceedings of SPIE Vol. 7732, 77324T, 2009.
15. Siegmund, O.H.W., J.B. McPhate, J.V. Vallerga, A.S. Tremsin, S.R. Jelinsky, H.J. Frisch, and the LAPPD Collaboration "Novel large format sealed tube microchannel plate detectors for Cherenkov timing and imaging" *Nuclear Instruments and Methods in Physics Research Section A*, in press 2010.
16. Siegmund O.H.W., J.V. Vallerga, A. Martin, B. Feller, M. Arif. D. Hussey, and D. Jacobsen, A high spatial resolution event counting neutron detector using microchannel plates and cross delay line readout, *Nucl. Instr. & Meth. A*, 579, 188-191, 2006
17. A. S. Tremsin, O. H. W. Siegmund, J. V. Vallerga, J. Hull, *IEEE Trans. Nucl. Sci.* **51**, pp.1707-1711, 2004
18. O.H.W. Siegmund, A. Tremsin, J.V. Vallerga, J. McPhate, Microchannel plate cross strip detectors with high spatial and temporal resolution, Nuclear Instruments and Methods, in press 2009
19. Colyer, R., Siegmund, O., Tremsin, A., Vallerga, J., Weiss, S., Michalet, X. Phasor-based single-molecule fluorescence lifetime imaging using a wide-field photon-counting detector, Proc. SPIE, Vol. 7185, p.14, 2009.
20. Michalet, X, Colyer, R, Siegmund, O, Tremsin, A, Vallerga, J, Weiss, S, H33D Gen II: A New Photon Counting Camera for Single-Molecule Imaging and Spectroscopy, Biophysical Journal, Vol. 98. p.761, 2010.
21. Leskelä Markku; Mikko Ritala. Atomic Layer Deposition Chemistry: Recent Developments and Future Challenges. Angew. Chem. Int. Ed. 42:, 2003.
22. Fraser G.W. X-ray detectors in astronomy Cambridge University Press, 1989,